



# Breather-like, singular, periodic, interaction of singular and periodic solitons, and a-periodic solitons of third-order nonlinear Schrödinger equation with an efficient algorithm

Jun Pan<sup>1,a</sup>, Mati Ur Rahman<sup>2,3,b</sup>, Rafiullah<sup>4,c</sup> 

<sup>1</sup> School of Foundation Studies, Zhejiang Pharmaceutical University, Ningbo Zhejiang 315500, China

<sup>2</sup> School of Mathematical Sciences, Jiangsu University, Zhenjiang 212013, Jiangsu, People's Republic of China

<sup>3</sup> Department of computer science and mathematics, Lebanese American university, Beirut, Lebanon

<sup>4</sup> Department of Mathematics, University of Swat, 01923 Swat, Khyber Pakhtunkhwa, Pakistan

Received: 8 June 2023 / Accepted: 27 September 2023

© The Author(s), under exclusive licence to Società Italiana di Fisica and Springer-Verlag GmbH Germany, part of Springer Nature 2023, corrected publication 2023

**Abstract** In this study, a diverse range of optical soliton solutions for the high-order nonlinear Schrödinger equation (NLSE) are discovered using the Sardar sub-equation (SSE) technique. Initially, we present the general algorithm for the SSE technique. Next, we employ the traveling wave transform on the proposed equation, transforming it into nonlinear ordinary differential (NLOD) equations. These NLOD equations are then separated into their real and imaginary components. Furthermore, we apply the proposed method to obtain new optical soliton solutions for the NLSE, including breather-like solitons, singular optical solitons, periodic solitons, the interaction of singular and periodic solitons, and a-periodic solitons. The study involves numerical simulations of the exact analytical optical soliton solutions, allowing for an exploration of the effects of various parameters on the soliton wave.

## 1 Introduction

In present era, multiple complex partial differential equations that are also known as nonlinear Schrödinger equations are studied by many researchers, which resulted in essential comprehensions to nonlinear pulses in optical fibers. These equations are a type of nonlinear PDEs and have been extensively investigated by researchers across a broad range of physical sciences. Partial differential equations known as nonlinear Schrödinger equations (NLSEs) appear in various areas of applied science as well as engineering, including but not limited to magneto static spin waves, optics, plasma physics, optical fibers, quantum mechanics, molecular biology, elastic media and fluid dynamics. These equations play a crucial role in modeling and understanding complex phenomena in these fields. For instance, new solitary solutions of complex Ginzburg–Landau model are studied in [1]. Multiple explicit exact solutions to the double-chain DNA dynamical system are reported in [2]. Different types of periodic solutions of new (3+ 1)-dimensional Boiti–Leon–Manna–Pempinelli equation are presented [3], Solving Local Time Fractional Telegraph Equations are demonstrated in [4].

Differential equations are very useful in describing the real-world phenomena including solitary waves solutions as well as fluid flow. Several researchers have worked in fluid mechanics, including ternary nanofluid, micropolar nanofluid, etc. For example new local and nonlocal solitary solutions of a nonlocal mKdV equation are observed in [5]. Resonance and fission/fusion solitons are presented in [6]. Besides these the numerical analysis of magneto-radiated annular fin natural convective heat transfer performance are reported in [7, 8]. Brownian motion and thermophoretic diffusion in bioconvective micropolar nanofluid flow are demonstrated in [9]. Numerical simulations of the temperature distribution of heat flow are presented in [10]. Heat transfer analysis of fractional model of couple stress Casson tri-hybrid nanofluid and conformable fluid mechanics model is studied in [11, 12]. Xu et al. studied bifurcation in a delayed chemostat model [13]. Further, predator–prey systems in fractional perspective is analyzed in [14, 15], chemical reaction models are studied in [16, 17] and bifurcations in fractional order BAM neural networks [18]. Similarly, SIR epidemic model is analyzed in [19], financial bubble mathematical model [20] and others [21].

Various researchers have delved into the study of NLS equations. As an illustration, efficient technique was employed by Biswas et al. for exploration of optical solitons in Schrödinger equation with nonlinear disturbance and resonance [22]. By the applications of fractional order singular as well as non-singular kernels the NLSE is studied in [23]. Hosseini et al. explored unstable NLSEs equations by Kudryashov method to obtain precise solutions in the form of traveling waves [24]. The extended tanh method was

<sup>a</sup> e-mail: [panpanjun\\_01@163.com](mailto:panpanjun_01@163.com)

<sup>b</sup> e-mail: [matimaths374@gmail.com](mailto:matimaths374@gmail.com)

<sup>c</sup> e-mail: [rafiswat999@gmail.com](mailto:rafiswat999@gmail.com) (corresponding author)

employed by Osman et al. to obtain soliton solutions for NLSE that incorporates time-dependent coefficients [25]. Soliton solutions for a nonlocal type NLSE were obtained by Kudryashov through the utilization of the simplest equation method [26]. Numerous scholars have directed their research efforts toward the domain of optical fiber communication systems. The study of solitons in fiber optics is a captivating and aesthetically pleasing area of research within the field of dynamical systems. Typically, the time-related aspects of these systems are emphasized and presented when they are analyzed or represented. These systems are examined with regard to their behavior and characteristics over time and analyzed through the transmission of the field at various frequencies. Dynamical systems, which are often in the form of complex nonlinear PDEs, have been extensively studied in this field [9, 11, 8]. Fiber amplifiers, nonlinear optical effects, and optical solitons have drastically improved long-distance data transmission, including undersea cables, leading to significant progress in the field. Researchers have also linked discrete breathers with embedded solitons, demonstrating the interaction between these two essential solution classes for the nonlinear Schrödinger equation. These solutions have attracted widespread attention from scientists and can explain various complex nonlinear phenomena. Following the development of NLSEs, the quest for exact solutions has been a major focus, with intensive exploration in various forms and facets. To obtain traveling wave solutions in diverse forms, numerous effective and potent methods have been utilized. These include the rational expansion scheme [30], semi-inverse variational principle [31], similarity transformations method [32], F-expansion method [33], Darboux transformation [34], direct algebraic technique [35], Jacobi elliptic function technique [36], expansion method [38], simple equation method [39] and many more methods are introduced. The comprehensive third-order NLSE, that belongs to the class of NLSEs, has recently received considerable attention. Its mathematical representation is as follow:

$$i \left( \frac{\partial \mathfrak{W}}{\partial t} + \frac{\partial^3 \mathfrak{W}}{\partial x^3} \right) + |\mathfrak{W}|^2 \left( \alpha_1 \mathfrak{W} + \alpha_2 \frac{\partial \mathfrak{W}}{\partial x} \right) + i \alpha_3 \frac{\partial |\mathfrak{W}|^2 \mathfrak{W}}{\partial x} = 0. \tag{1}$$

The coefficients of nonlinear dispersions are represented by  $\alpha_j$ ,  $j = 1, 2, 3$ , and the coefficient  $\alpha_1$  corresponds to the cubic nonlinearity term in the equation. When  $\alpha_1$  and  $\alpha_3$  are equal to zero, the above model simplifies to the Hirota or modified KdV equation in complex form. This simplified equation can be solved using the inverse scattering transform. Several effective methods have been employed to solve the nonlinear model mentioned above, which is used for modeling ultra-short pulses. For example, Lu et al. utilized both the extended simple equation method and the  $\exp(-f(\xi))$ -expansion method to demonstrate optical solitons in the model [40]. Using the generalized Riccati mapping method, Nasreen et al. identified different categories of soliton solutions for the model.

## 2 General analysis of the SSEM

In this section the steps of the suggested technique are presented. For the description of the method consider the following general nonlinear PDE:

$$\mathcal{Z}(\mathcal{B}, \mathcal{B}_t, \mathcal{B}_x, \mathcal{B}_{tt}, \mathcal{B}_{xx}, \mathcal{B}_t, \mathcal{B}_{tx}, ) = 0. \tag{2}$$

Further consider the following transformation

$$\mathcal{B}(x, t) = \exp(i\zeta) \mathfrak{A}(\delta), \quad \delta = \kappa x + \mathcal{C}t, \quad \zeta = \Lambda x + \theta + \lambda t, \tag{3}$$

in the above transformation  $\mathcal{C}$ ,  $\lambda$ ,  $\epsilon$  are real parameters, which are non-zero. Now to solve Eq.(2), the following are necessary to be followed:

*Step I:* Substitute Eq.(3) into Eq. 2, in order to convert the PDE to ODE and get the following form

$$\mathcal{Z}(\mathfrak{A}(\delta), \mathfrak{A}'(\delta), \mathfrak{A}''(\delta), \dots) = 0, \tag{4}$$

in Eq.(4), the  $\mathcal{Z}$  is polynomial in  $\mathfrak{A}(\delta)$ , where the superscripts ( $\prime$ ) represents ordinary derivatives of  $\mathfrak{A}(\delta)$ .

*Step II:* Consider that the ODE in Eq.(4) has solution in the following form

$$\mathfrak{A}(\delta) = \sum_{l=0}^{\epsilon} \varrho_l \mathcal{C}(\delta)^l, \quad \varrho_\epsilon \neq 0, \tag{5}$$

where  $\varrho_0, \varrho_1, \varrho_2, \dots, \varrho_\epsilon$  are real constants to be determined,  $\epsilon \in \mathbb{Z}^+$ . One can determine  $\epsilon$  by homogeneous balance principle by comparing highest power of nonlinearity and highest order of derivative. Further  $\mathcal{C}(\delta)$  satisfies the ODE presented below

$$\frac{d\mathcal{C}(\delta)}{d\delta} = \sqrt{\mathfrak{F}_1 + \mathfrak{F}_2 \mathcal{C}(\delta)^2 + \mathfrak{F}_3 \mathcal{C}(\delta)^4}. \tag{6}$$

Equation (6) has the solutions presented below:

Case I: When  $\mathfrak{F}_2 > 0$  and  $\mathfrak{F}_1 = 0$ , then

$$\begin{aligned} C_1^\pm(\delta) &= \pm\sqrt{-\mathcal{J}\mathcal{K}\mathfrak{F}_2} \operatorname{sech} \mathcal{J}\mathcal{K}(\sqrt{\mathfrak{F}_2}\delta) \\ C_2^\pm(\delta) &= \pm\sqrt{\mathcal{J}\mathcal{K}\mathfrak{F}_2} \operatorname{csc} h \mathcal{J}\mathcal{K}(\sqrt{\mathfrak{F}_2}\delta) \end{aligned} \tag{7}$$

here

$$\operatorname{sech} \mathcal{J}\mathcal{K}(\delta) = \frac{2}{\mathcal{J}e^\delta + \mathcal{K}e^{-\delta}}, \operatorname{csc} h \mathcal{J}\mathcal{K}(\delta) = \frac{2}{\mathcal{J}e^\delta - \mathcal{K}e^{-\delta}}. \tag{8}$$

Case II: When  $\mathfrak{F}_2 < 0$  and  $\mathfrak{F}_1 = 0$ , then

$$\begin{aligned} C_3^\pm(\delta) &= \pm\sqrt{-\mathcal{J}\mathcal{K}\mathfrak{F}_2} \operatorname{sec} \mathcal{J}\mathcal{K}(\sqrt{-\mathfrak{F}_2}\delta) \\ C_4^\pm(\delta) &= \pm\sqrt{-\mathcal{J}\mathcal{K}\mathfrak{F}_2} \operatorname{csc} \mathcal{J}\mathcal{K}(\sqrt{-\mathfrak{F}_2}\delta) \end{aligned} \tag{9}$$

here

$$\operatorname{sec} \mathcal{J}\mathcal{K}(\delta) = \frac{2}{\mathcal{J}e^{i\delta} + \nu e^{-i\delta}}, \operatorname{csc} \mathcal{J}\mathcal{K}(\delta) = \frac{2i}{\mathcal{J}e^{i\delta} - \nu e^{-i\delta}}. \tag{10}$$

Case III: When  $\mathfrak{F}_2 < 0$  and  $\mathfrak{F}_1 = \frac{\mathfrak{F}_2^2}{4}$ , then

$$\begin{aligned} C_5^\pm(\delta) &= \pm\sqrt{-\frac{\mathfrak{F}_2}{2}} \operatorname{tanh} \mathcal{J}\mathcal{K}(\sqrt{-\frac{\mathfrak{F}_2}{2}}\delta) \\ C_6^\pm(\delta) &= \pm\sqrt{-\frac{\mathfrak{F}_2}{2}} \operatorname{coth} \mathcal{J}\mathcal{K}(\sqrt{-\frac{\mathfrak{F}_2}{2}}\delta) \\ C_7^\pm(\delta) &= \pm\sqrt{-\frac{\mathfrak{F}_2}{2}} (\operatorname{tanh} \mathcal{J}\mathcal{K}(\sqrt{-2\mathfrak{F}_2}\delta) + i\sqrt{-\mathcal{J}\mathcal{K}} \operatorname{sec} h \mathcal{J}\mathcal{K}(\sqrt{-2\mathfrak{F}_2}\delta)) \\ C_8^\pm(\delta) &= \pm\sqrt{-\frac{\mathfrak{F}_2}{2}} (\operatorname{coth} \mathcal{J}\mathcal{K}(\sqrt{-2\mathfrak{F}_2}\delta) + \sqrt{-\mathcal{J}\mathcal{K}} \operatorname{csc} h \mathcal{J}\mathcal{K}(\sqrt{-2\mathfrak{F}_2}\delta)) \\ C_9^\pm(\delta) &= \pm\sqrt{-\frac{\mathfrak{F}_2}{2}} (\operatorname{coth} \mathcal{J}\mathcal{K}(\sqrt{-\frac{\mathfrak{F}_2}{8}}\delta) + i \operatorname{tanh} \mathcal{J}\mathcal{K}(\sqrt{-\frac{\mathfrak{F}_2}{8}}\delta)), \end{aligned} \tag{11}$$

here

$$\operatorname{tanh} \mathcal{J}\mathcal{K}(\delta) = \frac{\mathcal{J}e^\delta - \mathcal{K}e^{-\delta}}{\mathcal{J}e^\delta + \mathcal{K}e^{-\delta}}, \operatorname{coth} \mathcal{J}\mathcal{K}(\delta) = \frac{\mathcal{J}e^\delta + \mathcal{K}e^{-\delta}}{\mathcal{J}e^\delta - \mathcal{K}e^{-\delta}}. \tag{12}$$

Case IV: When  $\mathfrak{F}_2 > 0$  and  $\mathfrak{F}_1 = \frac{\mathfrak{F}_2^2}{4}$ , then

$$\begin{aligned} C_{10}^\pm(\delta) &= \pm\sqrt{\frac{\mathfrak{F}_2}{2}} \operatorname{tan} \mathcal{J}\mathcal{K}(\sqrt{\frac{\mathfrak{F}_2}{2}}\delta) \\ C_{11}^\pm(\delta) &= \pm\sqrt{\frac{\mathfrak{F}_2}{2}} \operatorname{cot} \mathcal{J}\mathcal{K}(\sqrt{\frac{\mathfrak{F}_2}{2}}\delta) \\ C_{12}^\pm(\delta) &= \pm\sqrt{\frac{\mathfrak{F}_2}{2}} (\operatorname{tan} \mathcal{J}\mathcal{K}(\sqrt{2\mathfrak{F}_2}\delta) + \sqrt{\mathcal{J}\mathcal{K}} \operatorname{sec} \mathcal{J}\mathcal{K}(\sqrt{2\mathfrak{F}_2}\delta)) \\ C_{13}^\pm(\delta) &= \pm\sqrt{\frac{\mathfrak{F}_2}{2}} (\operatorname{cot} \mathcal{J}\mathcal{K}(\sqrt{2\mathfrak{F}_2}\delta) + \sqrt{\mathcal{J}\mathcal{K}} \operatorname{csc} \mathcal{J}\mathcal{K}(\sqrt{2\mathfrak{F}_2}\delta)) \\ C_{14}^\pm(\delta) &= \pm\sqrt{\frac{\mathfrak{F}_2}{2}} \left( \operatorname{cot} \mathcal{J}\mathcal{K}(\sqrt{\frac{\mathfrak{F}_2}{8}}\delta) + i \operatorname{tan} \mathcal{J}\mathcal{K}(\sqrt{\frac{\mathfrak{F}_2}{8}}\delta) \right), \end{aligned} \tag{13}$$

here

$$\operatorname{tan} \mathcal{J}\mathcal{K}(\delta) = \frac{\mathcal{J}e^{i\delta} - \nu e^{-i\delta}}{\mathcal{J}e^{i\delta} + \nu e^{-i\delta}}, \operatorname{cot} \mathcal{J}\mathcal{K}(\delta) = \frac{\mathcal{J}e^{i\delta} + \nu e^{-i\delta}}{\mathcal{J}e^{i\delta} - \nu e^{-i\delta}}. \tag{14}$$

### 3 Application of the SSEM

Here we apply the suggested scheme to the proposed model and acquire several novel solutions. For this we substitute the following transformations into Eq.(1)

$$\mathcal{U}(x, t) = \exp(i\zeta)A(\delta), \delta = \kappa x + \mathcal{C}t, \zeta = \Lambda x + \theta + \lambda t. \tag{15}$$

The symbols  $\mathfrak{A}(\delta)$ ,  $\delta$  and  $\mathcal{C}$  are used to denote the soliton pulse profile, frequency, wave number and soliton velocity respectively. On substituting Eq.(15) into Eq.(1), we obtained the real and imaginary parts as

$$(\Lambda^3 - \lambda)\mathfrak{A}(\delta) - 3\Lambda\kappa^2\mathfrak{A}''(\delta) + \mathfrak{A}(\delta)^3(\alpha_1 - \Lambda(\alpha_2 + 2\alpha_3)) = 0. \tag{16}$$

$$\mathfrak{A}'(\delta)(\gamma - 3\Lambda^2\kappa + \kappa(\alpha_2 + 2\alpha_3)\mathfrak{A}(\delta)^2) + \kappa^3\mathfrak{A}'''(\delta) = 0. \tag{17}$$

Now integrating Eq.(16) once and considering the integration constant as zero, we obtained

$$\mathfrak{A}(\delta)(\gamma - 3\Lambda^2\kappa) + \kappa^3\mathfrak{A}''(\delta) + \frac{1}{3}\kappa(\alpha_2 + 2\alpha_3)\mathfrak{A}(\delta)^3 = 0, \tag{18}$$

comparing Eq.(16) and Eq.(18), we obtained the following constraint conditions

$$\lambda = -\gamma + \Lambda^3 + 3\Lambda^2\kappa; \alpha_2 = \frac{3\alpha_1 - 6\alpha_3\Lambda - 2\alpha_3\kappa}{3\Lambda + \kappa};$$

Using the homogeneous balance principle, we obtained the value of  $\mathfrak{E} = 1$ , so from Eq.(5), we have

$$\mathfrak{A}(\delta) = \varrho_0 + \varrho_1\mathcal{C}(\delta), \quad \varrho_1 \neq 0, \tag{19}$$

where in Eq.(19),  $\mathcal{C}(\delta)$  satisfies the following ODE

$$\frac{d\mathcal{C}(\delta)}{d\delta} = \sqrt{\mathfrak{F}_1 + \mathfrak{F}_2\mathcal{C}(\delta)^2 + \mathfrak{F}_3\mathcal{C}(\delta)^4}. \tag{20}$$

Further inserting Eq.(20) into Eq.(19) and then into Eq.(18), we get the algebraic system of equations which is as follows

$$\begin{aligned} \mathcal{C}(\delta)^0 : \varrho_0 \left( \gamma - 3\Lambda^2\kappa + \frac{\alpha_1\kappa\varrho_0^2}{3\Lambda + \kappa} \right) &= 0 \\ \mathcal{C}(\delta)^1 : \gamma - 3\Lambda^2\kappa - 3\Lambda\kappa^2\mathfrak{F}_2 + \frac{3\alpha_1\kappa\varrho_0^2}{3\Lambda + \kappa} &= 0 \\ \mathcal{C}(\delta)^2 : \frac{3\alpha_1\kappa\varrho_0\varrho_1^2}{3\Lambda + \kappa} &= 0 \\ \mathcal{C}(\delta)^3 : \kappa\varrho_1 \left( \frac{\alpha_1\varrho_1^2}{3\Lambda + \kappa} - 6\Lambda\kappa\mathfrak{F}_3 \right) &= 0. \end{aligned}$$

Solving the above system gives the following non-trivial values of parameters

$$\begin{aligned} \varrho_0 = 0, \varrho_1 &= \frac{\sqrt{6}\sqrt{3\Lambda^2\kappa\mathfrak{F}_3 + \Lambda\kappa^2\mathfrak{F}_3}}{\sqrt{\alpha_1}}, \mathfrak{F}_2 = \frac{\gamma - 3\Lambda^2\kappa}{3\Lambda\kappa^2} \\ \varrho_0 = 0, \varrho_1 &= -\frac{\sqrt{6}\sqrt{3\Lambda^2\kappa\mathfrak{F}_3 + \Lambda\kappa^2\mathfrak{F}_3}}{\sqrt{\alpha_1}}, \mathfrak{F}_2 = \frac{\gamma - 3\Lambda^2\kappa}{3\Lambda\kappa^2}. \end{aligned}$$

On substituting the above sets of parameter values into equations (7), (9), (11) and (13), we obtained the following exact solutions of the proposed perturbed NLSE

Case I: When  $\mathfrak{F}_2 > 0$  and  $\mathfrak{F}_1 = 0$ , then

$$U_1^\pm(x, t) = \pm\varrho_1\sqrt{-\mathcal{J}\mathcal{K}\mathfrak{F}_2} \exp(\iota\zeta) \operatorname{sech}_{\mathcal{J}\mathcal{K}} \left( \sqrt{\mathfrak{F}_2}(\kappa x - \mathcal{C}t) \right), \tag{21}$$

where the existence condition for the above solution is  $\mathcal{J}\mathcal{K} < 0$ .

$$U_2^\pm(x, t) = \pm\varrho_1\sqrt{\mathcal{J}\mathcal{K}\mathfrak{F}_2} \exp(\iota\zeta) \operatorname{csc}_{\mathcal{J}\mathcal{K}} \left( \sqrt{\mathfrak{F}_2}(\kappa x - \mathcal{C}t) \right), \tag{22}$$

where the existence condition for the above solution is  $\mathcal{J}\mathcal{K} > 0$ .

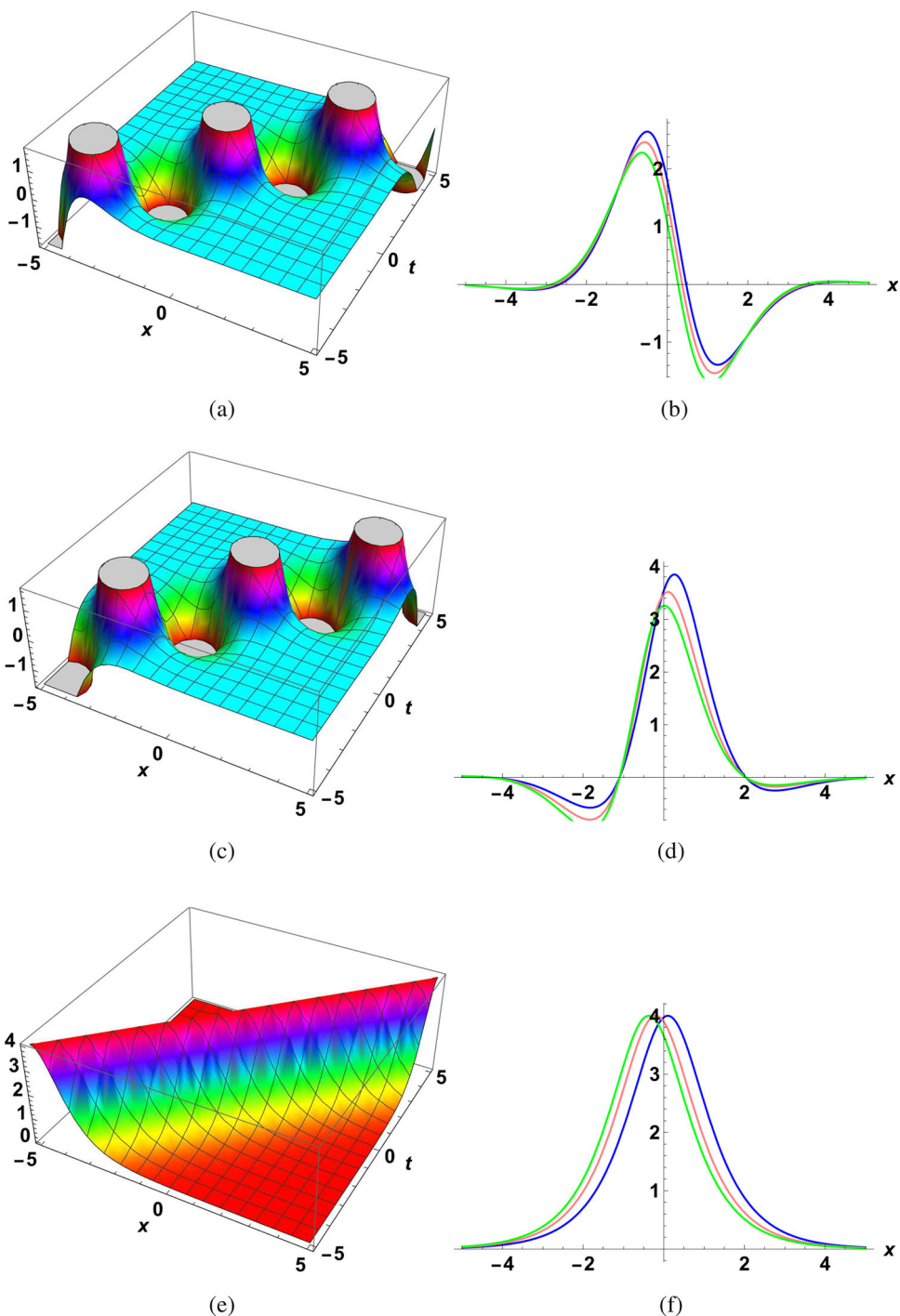
Case II: When  $\mathfrak{F}_2 < 0$  and  $\mathfrak{F}_1 = 0$ , then

$$U_3^\pm(x, t) = \pm\varrho_1\sqrt{-\mathcal{J}\mathcal{K}\mathfrak{F}_2} \exp(\iota\zeta) \operatorname{sec}_{\mathcal{J}\mathcal{K}} \left( \sqrt{-\mathfrak{F}_2}(\kappa x - \mathcal{C}t) \right), \tag{23}$$

$$U_4^\pm(x, t) = \pm\varrho_1\sqrt{\mathcal{J}\mathcal{K}\mathfrak{F}_2} \exp(\iota\zeta) \operatorname{csc}_{\mathcal{J}\mathcal{K}} \left( \sqrt{-\mathfrak{F}_2}(\kappa x - \mathcal{C}t) \right), \tag{24}$$

where the existence condition for the above solutions is  $\mathcal{J}\mathcal{K} > 0$ .

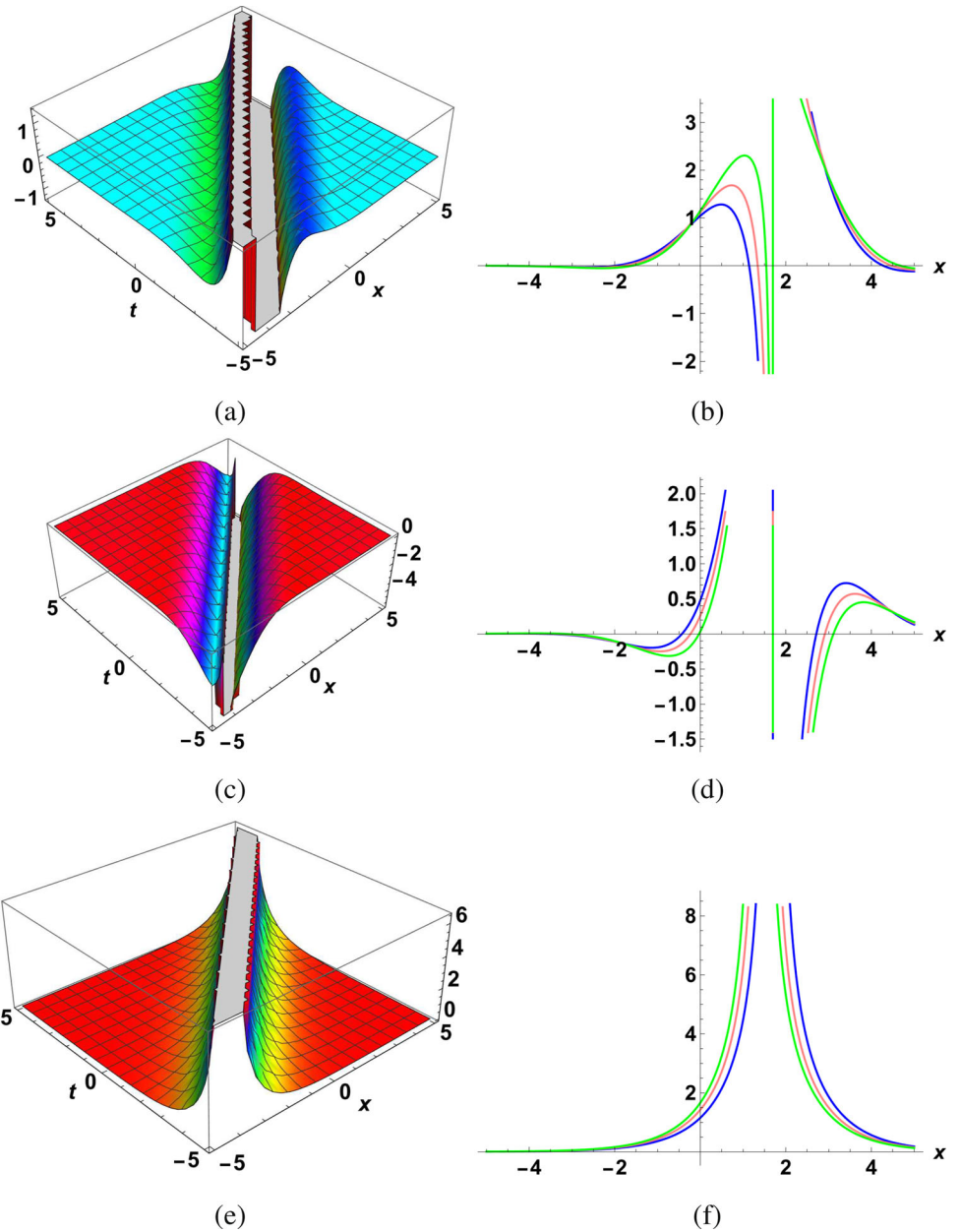
**Fig. 1** Visualization solution  $U_1(x, t)$  with parameters used in the form  $\Lambda = 1, \kappa = 1, \mathcal{C} = 1, \alpha_1 = 1, \mathcal{J} = -1, \varrho_3 = 1, \theta = 1, \lambda = 1, \mathcal{K} = 1$



Case III: When  $\mathfrak{F}_2 < 0$  and  $\mathfrak{F}_1 = \frac{\mathfrak{F}_2^2}{4}$ , then

$$\begin{aligned}
 U_5^\pm(x, t) &= \pm \varrho_1 \sqrt{-\frac{\mathfrak{F}_2}{2}} \exp(\iota \zeta) \tanh \mathcal{J} \mathcal{K} \left( \sqrt{-\frac{\mathfrak{F}_2}{2}} (\kappa x - \mathcal{C}t) \right), \\
 U_6^\pm(x, t) &= \pm \varrho_1 \sqrt{-\frac{\mathfrak{F}_2}{2}} \exp(\iota \zeta) \coth \mathcal{J} \mathcal{K} \left( \sqrt{-\frac{\mathfrak{F}_2}{2}} (\kappa x - \mathcal{C}t) \right), \\
 U_7^\pm(x, t) &= \pm \varrho_1 \sqrt{-\frac{\mathfrak{F}_2}{2}} \exp(\iota \zeta) (\tanh \mathcal{J} \mathcal{K} (\sqrt{-2\mathfrak{F}_2} (\kappa x - \mathcal{C}t)) + \iota \sqrt{\mathcal{J} \mathcal{K}} \operatorname{sech} \mathcal{J} \mathcal{K} (\sqrt{-2\mathfrak{F}_2} (\kappa x - \mathcal{C}t))), \\
 U_8^\pm(x, t) &= \pm \varrho_1 \sqrt{-\frac{\mathfrak{F}_2}{2}} \exp(\iota \zeta) (\coth \mathcal{J} \mathcal{K} (\sqrt{-2\mathfrak{F}_2} (\kappa x - \mathcal{C}t)) + \sqrt{\mathcal{J} \mathcal{K}} \operatorname{csc} h \mathcal{J} \mathcal{K} (\sqrt{-2\mathfrak{F}_2} (\kappa x - \mathcal{C}t))), \\
 U_9^\pm(x, t) &= \pm \varrho_1 \sqrt{-\frac{\mathfrak{F}_2}{2}} \exp(\iota \zeta) \left( \coth \mathcal{J} \mathcal{K} \left( \sqrt{-\frac{\mathfrak{F}_2}{8}} (\kappa x - \mathcal{C}t) \right) + \iota \tanh \mathcal{J} \mathcal{K} \left( \sqrt{-\frac{\mathfrak{F}_2}{8}} (\kappa x - \mathcal{C}t) \right) \right).
 \end{aligned} \tag{25}$$

**Fig. 2** Visualization solution  $\mathcal{U}_2(x, t)$  with parameters used in the form  $\Lambda = 1, \kappa = -1, \mathcal{C} = 1, \alpha_1 = 1, \mathcal{J} = 1, \varrho_3 = 1, \theta = 1, \lambda = -1, \mathcal{K} = 0.2$



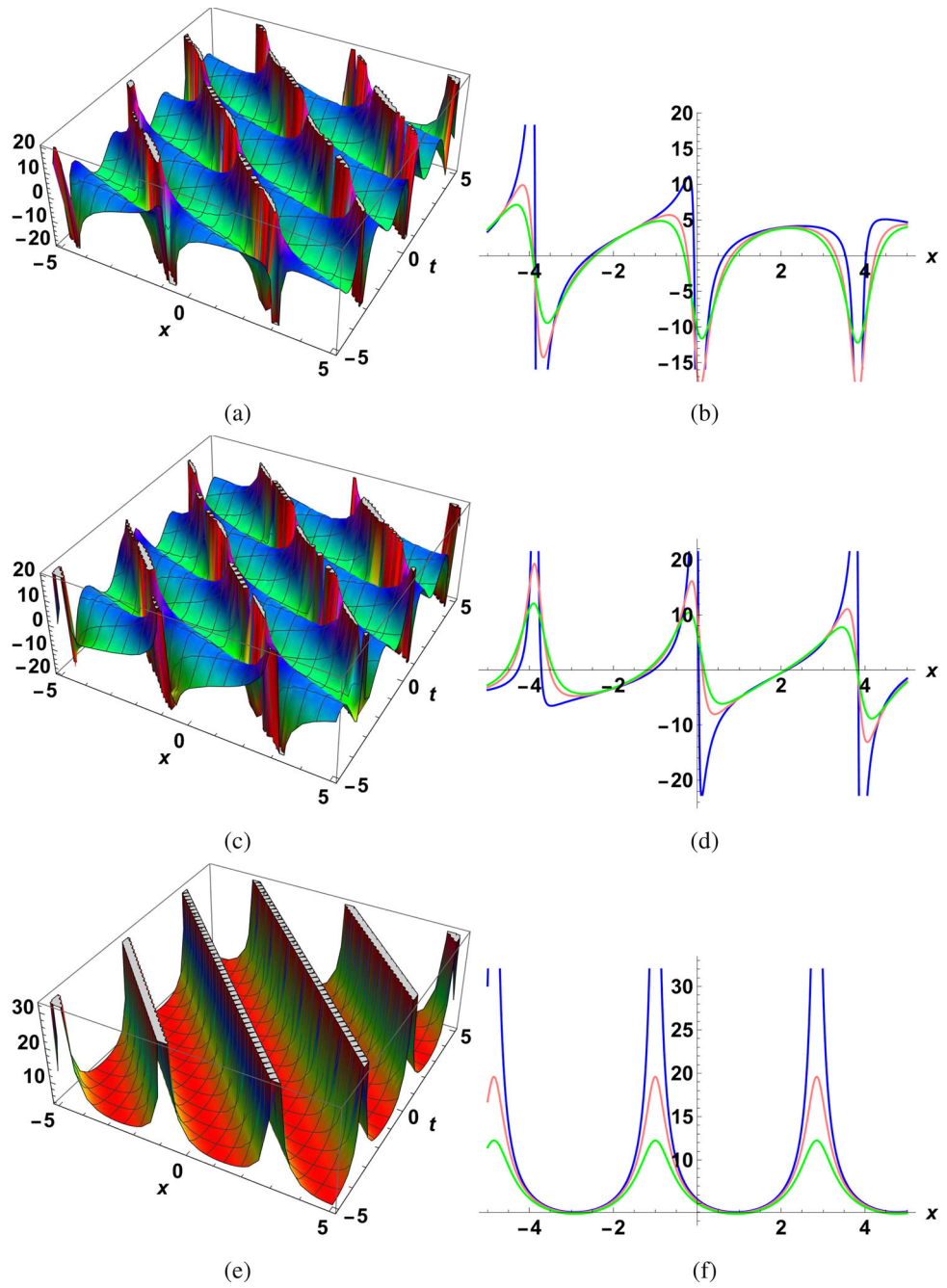
Case IV: When  $\mathfrak{F}_2 > 0$  and  $\mathfrak{F}_1 = \frac{\mathfrak{F}_2^2}{4}$ , then

$$\begin{aligned}
 \mathcal{U}_{10}^\pm(x, t) &= \pm \varrho_1 \sqrt{\frac{\mathfrak{F}_2}{2}} \exp(\iota \zeta) \tan \mathcal{J} \mathcal{K} \left( \sqrt{\frac{\mathfrak{F}_2}{2}} (\kappa x - \mathcal{C}t) \right), \\
 \mathcal{U}_{11}^\pm(x, t) &= \pm \varrho_1 \sqrt{\frac{\mathfrak{F}_2}{2}} \exp(\iota \zeta) \cot \mathcal{J} \mathcal{K} \left( \sqrt{\frac{\mathfrak{F}_2}{2}} (\kappa x - \mathcal{C}t) \right), \\
 \mathcal{U}_{12}^\pm(x, t) &= \pm \varrho_1 \sqrt{\frac{\mathfrak{F}_2}{2}} \exp(\iota \zeta) \left( \tan \mathcal{J} \mathcal{K} \left( \sqrt{2\mathfrak{F}_2} (\kappa x - \mathcal{C}t) \right) + \sqrt{\mathcal{J} \mathcal{K}} \sec \mathcal{J} \mathcal{K} \left( \sqrt{2\mathfrak{F}_2} (\kappa x - \mathcal{C}t) \right) \right), \\
 \mathcal{U}_{13}^\pm(x, t) &= \pm \varrho_1 \sqrt{\frac{\mathfrak{F}_2}{2}} \exp(\iota \zeta) \left( \cot \mathcal{J} \mathcal{K} \left( \sqrt{2\mathfrak{F}_2} (\kappa x - \mathcal{C}t) \right) + \sqrt{\mathcal{J} \mathcal{K}} \csc \mathcal{J} \mathcal{K} \left( \sqrt{2\mathfrak{F}_2} (\kappa x - \mathcal{C}t) \right) \right), \\
 \mathcal{U}_{14}^\pm(x, t) &= \pm \varrho_1 \sqrt{\frac{\mathfrak{F}_2}{2}} \exp(\iota \zeta) \left( \cot \mathcal{J} \mathcal{K} \left( \sqrt{\frac{\mathfrak{F}_2}{8}} (\kappa x - \mathcal{C}t) \right) + \iota \tan \mathcal{J} \mathcal{K} \left( \sqrt{\frac{\mathfrak{F}_2}{8}} (\kappa x - \mathcal{C}t) \right) \right).
 \end{aligned}
 \tag{26}$$

All of the above equations are checked and they satisfy the considered perterbed NLSE.



**Fig. 3** Visualization solution  $\mathcal{U}_4(x, t)$  with parameters used in the form  $\mathcal{U}_4(x, t)$  with parameters used in the form  $\Lambda = 1, \kappa = 1, \mathcal{C} = 1, \alpha_1 = 1, \mathcal{J} = 1, \varrho_3 = 1, \theta = 1, \lambda = 3, \mathcal{H} = 1.1$

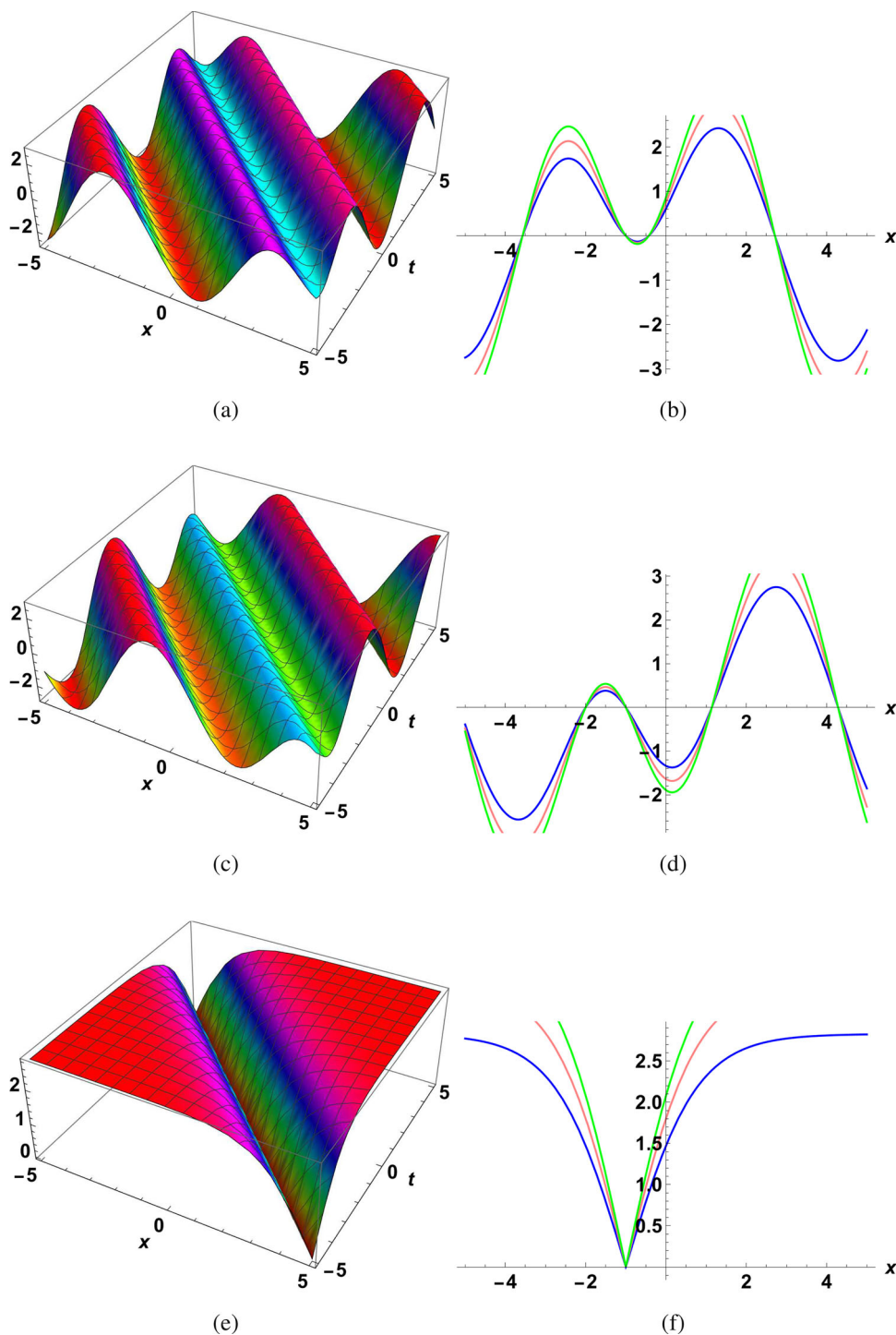


### 4 Simulations and discussions

This goal of this section is to presents the numerical simulations of some of the exact solutions obtained with the suggested technique of Eq.(1), which are given in equations (21)-(26). The presented figures contains six sub-plots, where the sub-plots (a), (c), (e) depict the 3D dynamics while (b), (d), (f) show the 2D dynamics of some of the exact solutions with suitable parameter values. The sub-plots [(a),(b)] in all figures show the real parts, [(c),(d)] demonstrate imaginary parts and [(e),(f)] show the absolute values of the solutions. Figure 1 shows the physical dynamics of solution  $\mathcal{U}_1(x, t)$ . The parameters in simulations of sub-figures [(a), (c), (e)] in Fig. 1 are considered as  $\Lambda = 1, \kappa = 1, \mathcal{C} = 1, \alpha_1 = 1, \mathcal{J} = -1, \varrho_3 = 1, \theta = 1, \lambda = 1, \mathcal{H} = 1$ . In sub-figures [(b), (d), (f)], the parameter  $\mathcal{H}$  is varied. The values are considered as for blue curve  $\mathcal{H} = 1$ , for pink curve  $\mathcal{H} = 2$  and for green curve  $\mathcal{H}$  is used as  $\mathcal{H} = 3$ , where we see that increasing  $\mathcal{H}$  decreases amplitudes of the waves.

Figure 2 portrays the evolution of solution  $\mathcal{U}_2(x, t)$ . The parameters during simulations of the sub-figures [(a), (c), (e)] in Fig. 2 are supposed to be  $\Lambda = 1, \kappa = -1, \mathcal{C} = 1, \alpha_1 = 1, \mathcal{J} = 1, \varrho_3 = 1, \theta = 1, \lambda = -1, \mathcal{H} = 0.2$ . In the sub-figures [(b),

**Fig. 4** Visualization solution  
 $\Lambda = 1, \kappa = 1, \mathcal{C} = 1, \alpha_1 = 1,$   
 $\mathcal{J} = 1, \varrho_3 = 1.1, \theta = 1,$   
 $\lambda = 0.9, \mathcal{K} = 1$



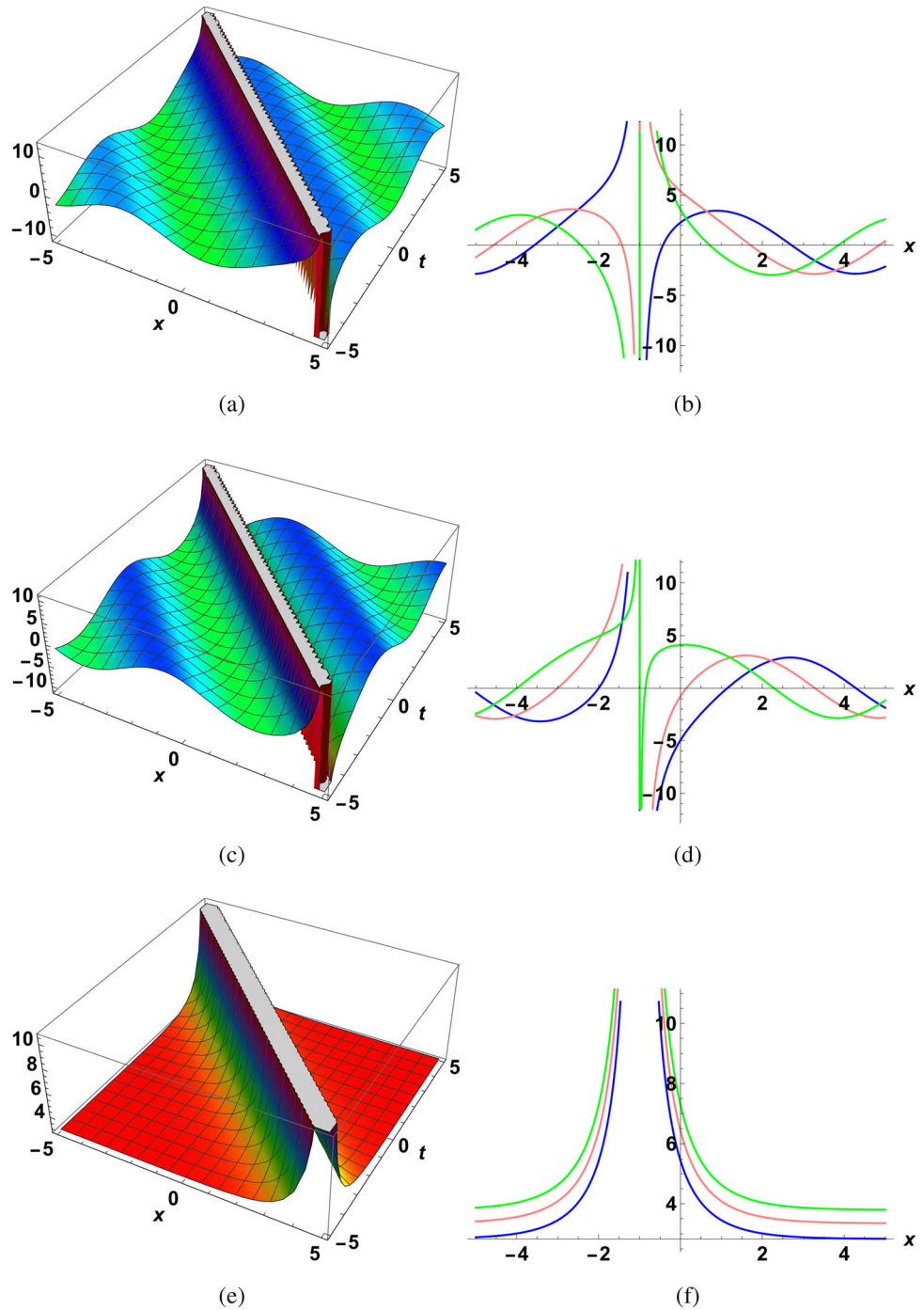
(d), (f)],  $\lambda$  is varied. The values are supposed as for the blue curve  $\lambda = 1$ , for pink curve  $\lambda = 0.8$ , for green curve  $\lambda$  is considered as  $\lambda = 0.6$  and  $t = 1$ , where one can see that decreasing  $\lambda$  increases the singular soliton's amplitude.

Figure 3 shows the physical demonstration of exact solution  $\mathcal{U}_4(x, t)$ . The parameters are supposed in the sub-figures [(a), (c), (e)] in Fig. 3 as  $\Lambda = 1, \kappa = 1, \mathcal{C} = 1, \alpha_1 = 1, \mathcal{J} = 1, \varrho_3 = 1, \theta = 1, \lambda = 3, \mathcal{K} = 1.1$ . Similarly in the sub-figures [(b), (d), (f)], different values of  $\gamma_3$  are considered. These are supposed as for the blue curve  $\mathcal{K} = 1.1$ , for the pink curve  $\mathcal{K} = 1.5$ , for the green curve  $\mathcal{K}$  is used as  $\mathcal{K} = 1.9$  and  $t = 0$ , where one can observe that increasing  $\mathcal{K}$  rapidly decreases the solitons' amplitudes.

Figures 4 and 5 depict the dynamic evolution of the solutions  $\mathcal{U}_5(x, t)$  and  $\mathcal{U}_6(x, t)$ , respectively. In the simulations of sub-figures [(a), (c), (e)] in Figs. 4 and 5, we consider the parameters as  $\Lambda = 1, \kappa = 1, \mathcal{C} = 1, \alpha_1 = 1, \mathcal{J} = 1, \varrho_3 = 1.1, \theta = 1, \lambda = 0.9, \mathcal{K} = 1$  and  $\Lambda = 1, \kappa = 1, \mathcal{C} = 1, \alpha_1 = 1, \mathcal{J} = 1, \varrho_3 = 1.1, \theta = 1, \lambda = 0.9, \mathcal{K} = 1$  for Figs. 4 and 5, respectively.



**Fig. 5** Visualization solution  $\mathcal{P}_4(x, t)$  with parameters used in the form  $\Lambda = 1, \kappa = 1, \mathcal{C} = 1, \alpha_1 = 1, \mathcal{J} = 1, \varrho_3 = 1.1, \theta = 1, \lambda = 0.9, \mathcal{K} = 1$

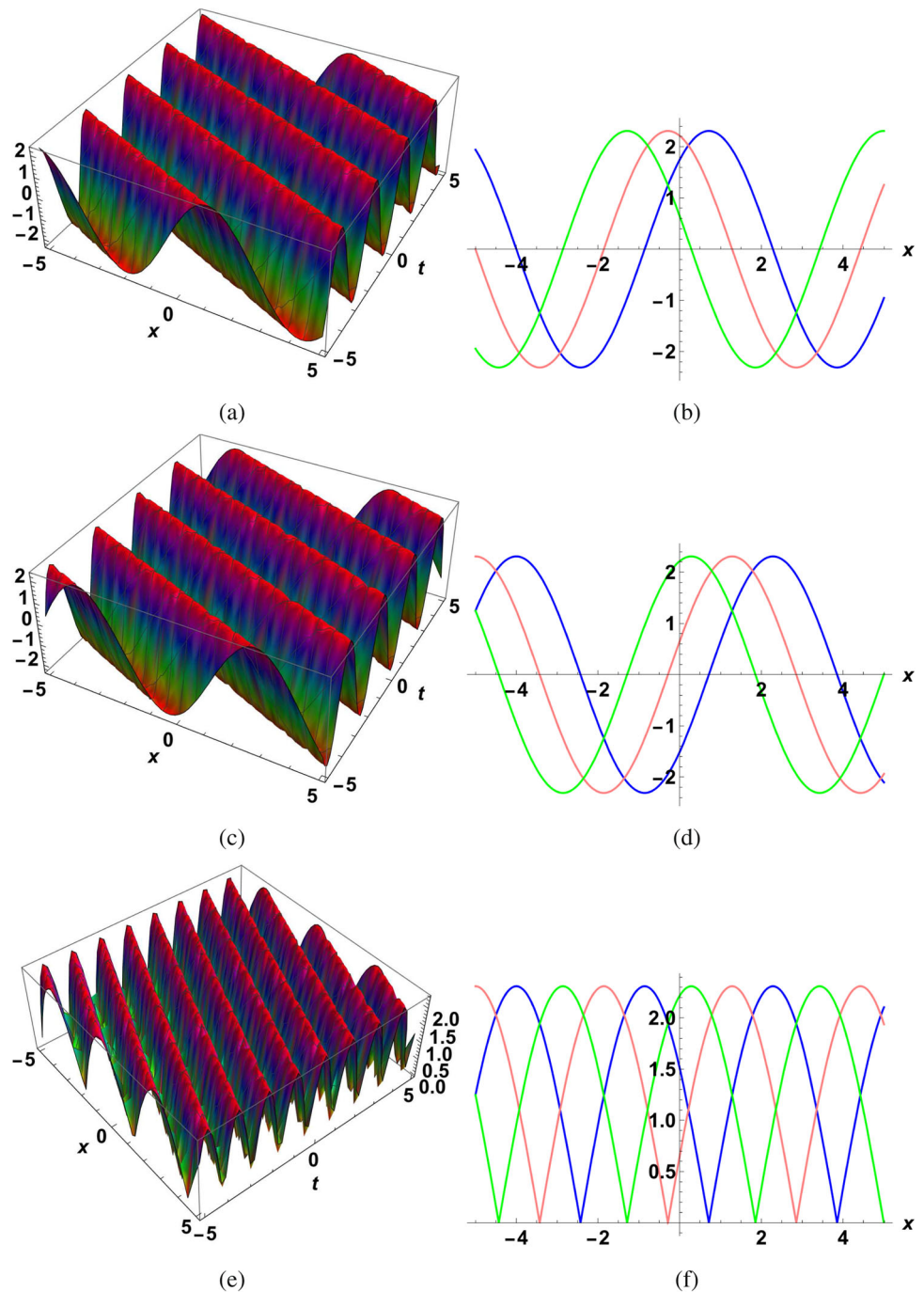


In sub-figures [(b), (d), (f)] of Fig. 4, we vary the parameter  $\varrho_3$ . Specifically, the blue curve corresponds to  $\varrho_3 = 1$ , the pink curve to  $\varrho_3 = 1.5$ , and the green curve to  $\varrho_3 = 2$  at  $t = 1$ . Observations reveal that decreasing  $\varrho_3$  amplifies the amplitudes of a-periodic solitons.

Similarly, for the sub-figures [(b), (d), (f)] of Fig. 5, we vary the parameter  $\theta$ . The values are set as follows: the blue curve represents  $\theta = 1$ , the pink curve  $\theta = 2$ , and the green curve  $\theta = 3$  at  $t = 1$ . It is observed that increasing  $\theta$  results in an increase in the amplitudes of hybrid singular periodic solitons.

During the simulation of Fig. 6, the parameters are considered as  $\Lambda = 1, \kappa = -1, \mathcal{C} = 1, \alpha_1 = -1, \mathcal{J} = 5, \varrho_3 = 1.7, \theta = 1.5, \lambda = 3.5, \mathcal{K} = 2.5$ , illustrating the dynamics of solution  $\mathcal{U}_7(x, t)$ . Furthermore, for the sub-figures [(b), (d), (f)] of Fig. 6, we vary the parameter  $\eta$ : The blue curve represents  $\lambda = 1.5$ , the pink curve  $\lambda = 2.5$ , and the green curve  $\lambda = 3.5$  at  $t = 1$ . It is observed that increasing  $\lambda$  displaces the locations of periodic solitons while maintaining constant amplitudes.

**Fig. 6** Visualization solution  $\mathcal{P}_4(x, t)$  with parameters used in the form  $\Lambda = 1, \kappa = -1, \mathcal{C} = 1, \alpha_1 = -1, \mathcal{J} = 5, \varrho_3 = 1.7, \theta = 1.5, \lambda = 3.5, \mathcal{K} = 2.5$



### 5 Conclusion

In summary, this study introduces an innovative approach to generate a diverse array of optical soliton solutions for the Nonlinear Schrödinger Equation (NLSE). The Sardar sub-equation (SSE) technique proves to be highly effective in obtaining precise analytical solutions for the NLSE. Initially, we applied a traveling wave transform to convert the NLSE into NLSE in both real and imaginary forms. Subsequently, through the expansion strategy of our proposed method, multiple soliton solutions are derived, including breather-like solitons, singular optical solitons, periodic solitons, the interaction of singular and periodic solitons, and a-periodic solitons. These solutions have significant implications across various applications.

Breather-like solitons, characterized by periodic oscillations, are valuable for robustly transmitting information over extended distances. Singular optical solitons, featuring infinite intensity at their center, find application in generating high-intensity laser pulses for precision cutting and welding. Periodic solitons, repeating at regular intervals, are pivotal in frequency combs for optical

communication and metrology. The interplay between singular and periodic solitons can create complex light patterns for optical switches and other devices. Lastly, a-periodic solitons, lacking periodicity, have been utilized in creating nonlinear optical fibers for amplifying and manipulating light signals.

In conclusion, solitons encompass a broad spectrum of applications in optics, spanning from fundamental research to practical applications in telecommunications, sensing, and manufacturing.

**Data Availability** No Data associated in the manuscript.

## References

1. H. Rezazadeh, New solitons solutions of the complex Ginzburg-Landau equation with Kerr law nonlinearity. *Optik* **167**, 218–227 (2018)
2. U. Younas, J. Ren, L. Akinyemi, H. Rezazadeh, On the multiple explicit exact solutions to the double-chain DNA dynamical system. *Math Meth Appl Sci* **46**(6), 6309–6323 (2023)
3. J.M. Qiao, R.F. Zhang, R.X. Yue, H. Rezazadeh, A.R. Seadawy, Three types of periodic solutions of new (3+ 1)-dimensional Boiti-Leon-Manna-Pempinelli equation via bilinear neural network method. *Math Meth Appl Sci* **45**(9), 5612–5621 (2022)
4. Y.M. Chu, M. Jneid, A. Chaouk, M. Inc, H. Rezazadeh, A. Houwe, Local time fractional reduced differential transform method for solving local time fractional telegraph equations. *Fractals* (2023). <https://doi.org/10.1142/S0218348X2340128X>
5. S. Ahmad, S. Saifullah, A. Khan, Mustafa Inc, New local and nonlocal soliton solutions of a nonlocal reverse space-time mKdV equation using improved Hirota bilinear method. *Phys Lett A* **450**, 128393 (2022)
6. S. Ahmad, S. Saifullah, A. Khan, A.M. Wazwaz, Resonance, fusion and fission dynamics of bifurcation solitons and hybrid rogue wave structures of Sawada-Kotera equation. *Commun Nonlinear Sci Num Simul* **119**, 107117 (2023)
7. N.A. Shah, I. Ahmed, K.K. Asogwa, A.A. Zafar, W. Weera, A. Akgül, Numerical study of a nonlinear fractional chaotic Chua's circuit. *Aims Math* **8**, 1636–1655 (2022)
8. M.M. AlBaidani, N.K. Mishra, M.M. Alam, S.M. Eldin, A.A. Alzahrani, A. Akgül, Numerical analysis of magneto-radiated annular fin natural-convective heat transfer performance using advanced ternary nanofluid considering shape factors with heating source. *Case Stud Therm Eng* **44**, 102825 (2023)
9. A. Shahzad, M. Imran, M. Tahir, S.A. Khan, A. Akgül, S. Abdullaev, C. Park, H.Y. Zahran, I.S. Yahia, Brownian motion and thermophoretic diffusion impact on Darcy-Forchheimer flow of bioconvective micropolar nanofluid between double disks with Cattaneo-Christov heat flux. *Alexan Eng J* **62**, 1–15 (2023)
10. F.K. Iyanda, H. Rezazadeh, M. Inc, A. Akgül, I.M. Bashiru, M.B. Hafeez, M. Krawczuk, Numerical simulation of temperature distribution of heat flow on reservoir tanks connected in a series. *Alexan Eng J* **66**, 785–795 (2023)
11. M. Arif, L. Di Persio, P. Kumam, W. Watthayu, A. Akgül, Heat transfer analysis of fractional model of couple stress Casson tri-hybrid nanofluid using dissimilar shape nanoparticles in blood with biomedical applications. *Sci Rep* **13**(1), 4596 (2023)
12. M.I. Liaqat, A. Akgül, M. De la Sen, M. Bayram, Approximate and exact solutions in the sense of conformable derivatives of quantum mechanics models using a novel algorithm. *Symmetry* **15**(3), 744 (2023)
13. X. Changjin, Q. Cui, Z. Liu, O.Y. Pan, X. Cui, M. Wei, U. Rahman, M. Farman, S. Ahmad, A. Zeb, Extended hybrid controller design of bifurcation in a delayed chemostat model, *MATCH Communications in Mathematical and in Computer. Chemistry* **90**(3), 609–648 (2023)
14. X. Changjin, M. Dan, Y. Pan, C. Aouiti, L. Yao, Exploring bifurcation in a fractional-order predator-prey system with mixed delays. *J Appl Anal Comput* **13**(3), 1119–1136 (2023). <https://doi.org/10.11948/20210313>
15. C.J. Xu, X.H. Cui, P.L. Li, J.L. Yan, L.Y. Yao, Exploration on dynamics in a discrete predator-prey competitive model involving time delays and feedback controls. *J Biol Dyn* **17**(1), 2220349 (2023)
16. C. Xu, D. Mu, Z. Liu, Y. Pang, M. Liao, P. Li, Bifurcation dynamics and control mechanism of a fractional-order delayed Brusselator chemical reaction model. *MATCH Commun Math Comput Chem* **89**(1), 73–106 (2023)
17. M. Dan, X. Changjin, Z. Liu, Y. Pang, Further insight into bifurcation and hybrid control tactics of a chlorine dioxide-iodine-malonic acid chemical reaction model incorporating delays. *MATCH Commun Math Comput Chem* **89**(3), 529–566 (2023)
18. P.L. Li, Y.J. Lu, C.J. Xu, J. Ren, Insight into Hopf bifurcation and control methods in fractional order BAM neural networks incorporating symmetric structure and delay. *Cognit Comput* (2023). <https://doi.org/10.1007/s12559-023-10155-2>
19. B. Li, Z. Eskandari, Dynamical analysis of a discrete-time SIR epidemic model. *J Franklin Inst* **360**(12), 7989–8007 (2023)
20. B. Li, T. Zhang, C. Zhang, Investigation of financial bubble mathematical model under fractal-fractional Caputo derivative. *FRACTALS (fractals)* **31**(05), 1–13 (2023)
21. Q. He, X. Zhang, P. Xia, C. Zhao, S. Li, A comparison research on dynamic characteristics of Chinese and American energy prices. *J Global Inf Manag (JGIM)* **31**(1), 1–16 (2023)
22. A. Biswas, Y.Yildirim, E. Yasar, Q. Zhou, S. P. Moshokoa, Milivoj Belic, Optical soliton perturbation with resonant nonlinear Schrödinger's equation having full nonlinearity by modified simple equation method. *Optik* **160**, 33–43 (2018)
23. A. Khan, A. Ali, S. Ahmad, S. Saifullah, K. Nonlaopon, A. Akgül, Nonlinear Schrödinger equation under non-singular fractional operators: A computational study. *Result Phys* **43**, 106062 (2022)
24. K. Hosseini, D. Kumar, M. Kaplan, E. Yazdani Bejarbaneh, New exact traveling wave solutions of the unstable nonlinear Schrödinger equations. *Commun Theor Phys* **68**(6), 761 (2017)
25. M.S. Osman, K. K. Ali, J.F. Gómez-Aguilar, A variety of new optical soliton solutions related to the nonlinear Schrödinger equation with time-dependent coefficients. *Optik* **222**, 165389 (2020)
26. N.A. Kudryashov, Solitary waves of the non-local Schrödinger equation with arbitrary refractive index. *Optik* **231**, 166443 (2021)
27. A. R. Seadawy, J. Wang, Modified KdV-Zakharov-Kuznetsov dynamical equation in a homogeneous magnetised electron-positron-ion plasma and its dispersive solitary wave solutions. *Pramana* **91**, 1–13 (2018)
28. D. Sinha, P. K. Ghosh, Integrable nonlocal vector nonlinear Schrödinger equation with self-induced parity-time-symmetric potential. *Phys Lett A* **381**(3), 124–128 (2017)
29. A. R. Seadawy, K. El-Rashidy, Nonlinear Rayleigh-Taylor instability of the cylindrical fluid flow with mass and heat transfer. *Pramana* **87**, 1–9 (2016)
30. X. Zeng, D.-S. Wang, A generalized extended rational expansion method and its application to (1+ 1)-dimensional dispersive long wave equation. *Appl Math Comput* **212**(2), 296–304 (2009)

31. A. R. Seadawy, Nonlinear wave solutions of the three-dimensional Zakharov-Kuznetsov-Burgers equation in dusty plasma. *Phys A Statist Mech Appl* **439**, 124–131 (2015)
32. M. Kumar, A. K. Tiwari, R. Kumar, Some more solutions of Kadomtsev-Petviashvili equation. *Comput Math Appl* **74**(10), 2599–2607 (2017)
33. Y. Yıldırım, Optical solitons with Biswas-Arshed equation by F-expansion method. *Optik* **227**, 165788 (2021)
34. X. Geng, J. Shen, B. Xue, A new nonlinear wave equation: Darboux transformation and soliton solutions. *Wave Motion* **79**, 44–56 (2018)
35. A.R. Seadawy, M. Arshad, L. Dianchen, Stability analysis of new exact traveling-wave solutions of new coupled KdV and new coupled Zakharov-Kuznetsov systems. *Euro Phys J Plus* **132**, 1–19 (2017)
36. A.H. Khater, A.R. Seadawy, M.A. Helal, General soliton solutions of an n-dimensional nonlinear Schrödinger equation. *Nuovo Cimento B* **115**(11), 1303–1311 (2000)
37. N.A. Kudryashov, M.B. Soukharev, M.V. Demina, Elliptic traveling waves of the Olver equation. *Commun Nonlinear Sci Num Simul* **17**(11), 4104–4114 (2012)
38. A.M.S. Kumar, J.P. Prasanth, V.M. Bannur, Quark-gluon plasma phase transition using cluster expansion method. *Phys A Statist Mech Appl* **432**, 71–75 (2015)
39. M. Arshad, A.R. Seadawy, L. Dianchen, Exact bright-dark solitary wave solutions of the higher-order cubic-quintic nonlinear Schrödinger equation and its stability. *Optik* **138**, 40–49 (2017)
40. D. Lu, A.R. Seadawy, J. Wang, M. Arshad, U. Farooq, Soliton solutions of the generalised third-order nonlinear Schrödinger equation by two mathematical methods and their stability. *Pramana* **93**, 1–9 (2019)
41. N. Nasreen, A.R. Seadawy, L. Dianchen, W.A. Albarakati, Dispersive solitary wave and soliton solutions of the generalized third order nonlinear Schrödinger dynamical equation by modified analytical method. *Result Phys* **15**, 102641 (2019)

Springer Nature or its licensor (e.g. a society or other partner) holds exclusive rights to this article under a publishing agreement with the author(s) or other rightsholder(s); author self-archiving of the accepted manuscript version of this article is solely governed by the terms of such publishing agreement and applicable law.